Coupling between pressure solution creep and diffusive mass transport in porous rocks

Elisabeth Gundersen, François Renard, Dag Kristian Dysthe, Knut Bjørlykke, Bjørn Jamtveit

HAL Id: insu-03607065
https://hal-insu.archives-ouvertes.fr/insu-03607065

Submitted on 13 Mar 2022

Coupling between pressure solution creep and diffusive mass transport in porous rocks

Elisabeth Gundersen,[1] François Renard,[1,2] Dag Kristian Dysthe,[1] Knut Bjørlykke,[1] and Bjørn Jamtveit[1]

[1] Pressure solution is widely regarded as a mechanism of ductile deformation in the upper crust. It is driven by stress differences and its rate is affected by temperature, grain size, and fluid chemistry. Pressure solution involves dissolution at grain contacts under high stress and precipitation at grain contacts on pore surfaces under low stress, leading to porosity reduction by precipitation in the pore space or by grain indentation. For a system closed at a grain scale, pressure solution is traditionally described by a mechanism involving three steps: (1) dissolution at intergranular interfaces, (2) diffusion of solutes inside the contact between two grains, and (3) precipitation on the surface of the grains in contact with the pore fluid. In this paper we propose a model where we have added a fourth step to this process, diffusive transport to other open pores, to account for the macroscopic diffusion of solutes in pore fluids, such that the deformation is not closed at the grain scale. In this model, differences in mineral solubility due to variations in stress and grain size produce concentration gradients which drive diffusive mass transport. The interaction between pressure solution at a grain scale and transport over distances of several grains can lead to the amplification of initial porosity heterogeneities and subsequent localization of deformation. Regions of intense dissolution compact and form "bands" in close proximity to regions where the porosity reduction is mainly due to cementation. Pressure solution augmented by large-scale diffusional transport will cause mass transport from fine-grained to coarse-grained rock volumes. We show that such processes are important during both diagenesis of sediments and compaction of fault gouge. *INDEX TERMS:* 3902 Mineral Physics: Creep and deformation; 5114 Physical Properties of Rocks: Permeability and porosity; 8045 Structural Geology: Role of fluids; 8159 Tectonophysics: Evolution of the Earth: Rheology—crust and lithosphere; *KEYWORDS:* cementation, compaction, diagenesis, gouge, pressure solution, transport

1. Introduction

[2] Pressure solution creep is a temperature- and stress-dependent deformation mechanism that modifies both the grain size and the porosity of rocks in the upper crust. As for elastic or plastic deformation, constitutive laws can describe deformation of rocks undergoing pressure solution through a viscoelastic model [*Schneider*, 1996], but the mechanisms operating at grain scales are not well understood, mainly because different mechanochemical processes interact during deformation. At the grain scale, the mechanochemical processes associated with pressure solution creep can be kinetically controlled by reactions at grain surface [*Oelkers et al.*, 1996] or diffusion-controlled by transport along grain boundaries [*Weyl*, 1959; *Rutter*, 1976; *Gratier and Guiguet*, 1986; *Cox and Paterson*, 1991; *Hickman and Evans*, 1991; *Spiers and Brzesowsky*, 1993]. In the following analysis we will show that the relative significance of interfacial kinetics and diffusional transport varies with time as a natural consequence of the mechanism of deformation itself.

[3] A simple mechanistic model describing pressure solution at a grain scale is water film diffusion, in which dissolution is assumed to take place at grain-to-grain contacts with the solutes diffusing along an adsorbed water film layer. The precipitation of the solutes then occurs on the pore surfaces [*Weyl*, 1959; *Rutter*, 1976], see Figure 1. The driving force for this deformation is the enhanced solubility at grain contacts due to the concentration of effective stress between grains. In this model, the grain boundary can be flat or it can have a geometry of channels and islands at a micron scale [*de Boer et al.*, 1977; *Spiers and Brzesowsky*, 1993; *Renard et al.*, 1999].

[4] The path of mass transport by diffusion is a critical factor in determining the rate-limiting step for pressure

[1] Fluid Rock Interaction Group, Departments of Geology and Physics, University of Oslo, Oslo, Norway.
[2] LGIT, Université J. Fourier, Grenoble, France.
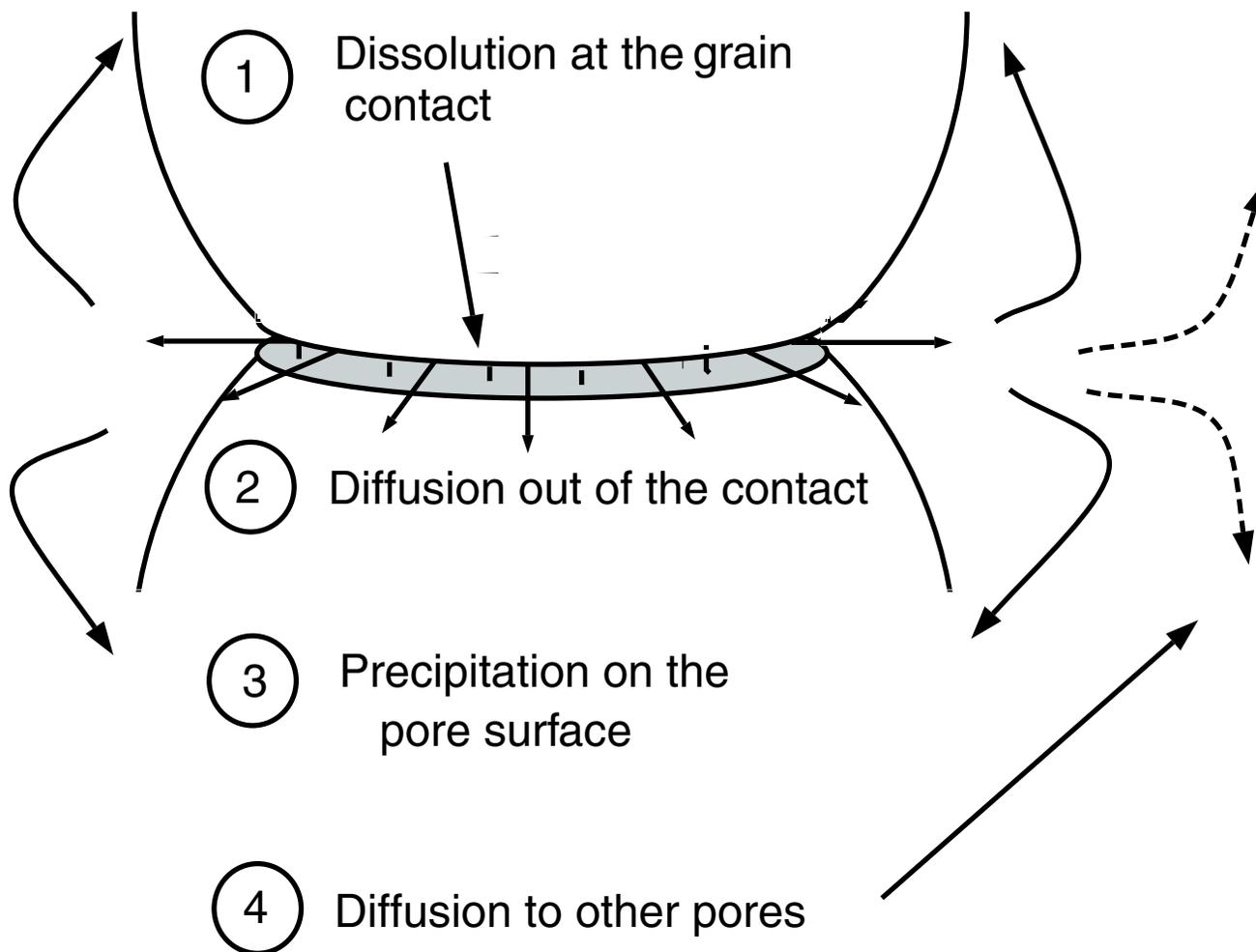
Figure 1. At a grain scale, pressure solution is a three-step process: (1) stress-enhanced dissolution at grain contacts, (2) diffusion along the contact to the pore, and (3) precipitation on the pore surface. If one considers that the system is not closed at the grain scale, a fourth step adds a level of complexity to the process: (4) transport between pores, which can lead to mass transport at decimeter or larger scales.

solution. For example, for the same effective stress, temperature, and fluid composition, the deformation of quartz aggregates via water film diffusion appears to be diffusion limited [*Gratier and Guiguet*, 1986] whereas the deformation of fluid inclusions via free fluid diffusion [*Gratier and Jenatton*, 1984] and the diagenesis of sandstones at shallow depths [*Oelkers et al.*, 1996, 2000] are limited by reaction kinetics. There is evidence which suggest that the rate of pressure solution of quartz/mica aggregates is limited by the quartz reaction kinetics at shallow (1–5 km) depth [*Bjørkum*, 1996; *Renard et al.*, 1997] and diffusion limited at greater depths [*Rutter*, 1976].

[5] In addition to variations in the mechanisms of pressure solution at grain scales, differences in compaction behavior may occur on a macroscopic scale, for example between sandstone beds within the same formation. Some layers may export silica whereas some other import it, this process is controlled by the variation of silica concentrations within each sandstone layer. *Trewin and Fallick* [2000] have observed that the Tumblagooda sandstone (Silurian, western Australia) contain layers where porosity decrease is due to cementation. These layers alternates with layers where

pressure solution at grain contacts appears to be responsible for the observed compaction.

[6] In the North Sea, quartz cement is the most pore-occluding mineral in deeply buried (>3000 m) sandstones [*Bjørlykke and Egeberg*, 1993]. In these and other oil-field sandstones, mechanochemical processes involved in diagenesis (cementation, pressure solution, etc.) appear to become important at temperatures above 90°C [*Worden and Morad*, 2000]. It is widely recognized that some of this quartz cement may be sourced by local pressure dissolution via quartz dissolution at highly stressed grain contacts.

[7] There is currently no consensus about the correlation between the grain size and extent of quartz cementation. Surface-reaction-controlled quartz precipitation would imply that finer grained sand should grow more quartz cement due to the larger surface area [*Walderhaug*, 1996]. However, some observations have suggested that most of the quartz cement is found between the coarser grains [*McBride*, 1989]. In this case, fine grains can dissolve faster due to the effect of grain size on solubility. In carbonate rocks, local transport of calcium carbonate from sites of pressure solution

to sites of cementations has been described by *Heidari and Moore* [1993] and *Heydari* [2000].

[8] In addition to these observations in a diagenetic context, mechanochemical processes also control the porosity and permeability evolution around active faults [*Evans and Chester*, 1995; *Janssen et al.*, 1997; *Renard et al.*, 2000]. The rates of mass transport and how fast such processes could cement the gouge and the walls of an active fault are still debated [*Hazidazeh and Foit*, 2000]. Furthermore, the driving force promoting this transport is not well-defined. Solutes could be transported over large distances by a circulating fluid or be transported over short distances within or adjacent to the fault zone by diffusion. Studies of exhumed faults indicate that mineralized veins are usually located within the gouge and in region of the fault walls directly in contact with the gouge [*Gaviglio et al.*, 1993; *Renard et al.*, 2000]. The mechanism underlying this localization of the cementation can be due to localized grain crushing in the gouge [*Mair and Marone*, 1999] and we believe also by a transport of mass enhanced by pressure solution, as discussed in this contribution.

[9] Numerical simulations have shown that small fluctuations in the initial porosity or grain size, in conjunction with pressure solution and diffusive mass transport in the pores, are sufficient to trigger an instability that causes layer-like patterns to develop in sandstones [*Merino et al.*, 1983; *Dewers and Ortoleva*, 1990]. This process needs only small initial variations that are amplified manifold during diagenesis. Diffusion along the open pores is a key factor because it controls how far solutes are transported to other locations. The relative effects of the diffusion and the dissolution/precipitation rates control the final geometry and spacing of these layers.

[10] The aim of this contribution is to establish a model of pressure solution, which is able to integrate both the deformation of single grains by pressure solution creep and the transport of solutes in the pores by diffusion. We apply this model to the three geological scenarios for which natural occurrences of pressure solution have already been described: amplification of a porosity or grain-size heterogeneity (concretions), amplification of layering in sedimentary rocks and cementation around a fracture containing a gouge.

2. Pressure Solution at a Grain Scale

[11] We will first consider the deformation at a grain scale (steps 1, 2, and 3 in Figure 1) and subsequently the transport of mass over distances larger than single grains (step 4).

2.1. Driving Force for Pressure Solution

[12] Deformation of grains by pressure solution is driven by a chemical potential gradient between the high-stress regions (i.e., the grain contacts) and the low-stress regions (in the pores) [*Kamb*, 1959; *Paterson*, 1973]. A Gibbs-type free energy cannot be defined for nonhydrostatically stressed solids [*Shimizu*, 1995], but the dissolution-precipitation reactions can be fully described by the surface chemical potential μ.

[13] The surface chemical potential is in general a tensor with components due to normal stress P, surface stress of an isotropic elastic solid, interfacial stress at curved interfaces and plastic defect distributions [*Heidug*, 1995; *Lehner*,

1995]. We choose to treat the grain contact region on a coarse scale where it turns out that only the normal stress at the grain contact contributes significantly. Readers seeking a less conceptual derivation are referred to the five references just cited.

[14] The chemical potential of a stressed solid is the sum of a temperature-dependent reference chemical potential at 1 bar, and a stress effect that depends on the stress normal to the solid surface P and the molar volume of the solid $\bar{V}_s$, the elastic energy contribution ΔU_e, a plastic energy contribution ΔU_d that takes in account the increase of energy due to crystal defects, and a surface energy term ΔU_γ that describes the increase of energy related to the radius of curvature of grains [*Paterson*, 1973].

$$\mu_{\text{solid}} = \mu_0(T) + \Delta P \bar{V}_s + \Delta U_d + \Delta U_e + \Delta U_\gamma \qquad (1)$$

where μ_0 is the chemical potential in a reference stress-free state. Taking the entire grain contact as the thermodynamic system we have chosen a coarse-grained description that does not include interface structure and connected high curvatures, local stress, etc. Although such structures at a smaller scale have been shown to have an impact on the large-scale rate laws of dissolution (D. K. Dysthe et al., Universal scaling during transient creep, submitted to *Geology*, 2002) the coarse graining is thermodynamically valid. Simple calculations using the coarse-grained description show that for most common geological conditions the effect of normal stress is two orders of magnitude higher than the four other effects [*Paterson*, 1973].

[15] The stress normal to the grain contact can be expressed as the macroscopic effective normal stress normalized by the surface area of the grain that supports the applied stress [*Dewers and Ortoleva*, 1990]. The stress normal to the free face of the grain is given by the fluid pressure. The difference between the stress at grain contacts and the pore fluid pressure, which evolves with depth and deformation, is the driving force for pressure solution. This difference of stress between the solid/grain-boundary fluid/solid contact and the free surfaces induces a chemical potential gradient that can be related to a concentration gradient if it is assumed that both the free fluid present in the open pores and the presumed fluid (or fluid-like) phase present in the intergranular contact region are in local equilibrium with the solid (or, at least, that the reaction rate is not zero). In the model, the stress normal to the z-contact is the overburden stress, the stress normal to x- and y-contacts is the main lateral stress.

[16] In addition to such potential gradients at grain scales, the presence of porosity or grain size heterogeneities can lead to potential gradients over distances larger than the grain size (step 4 in Figure 1). For example, at the interface between two sedimentary rock layers with identical mineralogy but with different porosity, a concentration gradient will develop in the pore fluid due to the variations in the normalized stress between the areas with different porosity. Moreover, in the higher porosity layer, the stress is more concentrated at grain contacts and pressure solution is more efficient than in the lower porosity layer. As a consequence, the grains tend to dissolve faster in the high porosity region; this process increases the concentration of solute in the pore fluid. The result is a diffusive transport in the pore fluid

from regions of higher concentration (and porosity) to regions of lower concentration. This process becomes more complex when, in addition to a porosity contrast, there is also a difference in grain size.

2.2. Properties of Water at Grain Contact

[17] We assume that a trapped water film exists between two mineral surfaces in contact. This film is stable, even if the effective stress, that is, the difference between the normal stress and the pore pressures, is large. For silica surfaces, it has been reported that the water film thickness decreases from 50 to 5 Å [*Pashley and Kitchener*, 1979; *Pashley and Israelachvili*, 1984; *Heidug*, 1995; *Renard and Ortoleva*, 1997] when the effective normal stress increases from 1 to 500 bars.

[18] An important factor to quantify pressure solution creep is the product of the water film thickness and the coefficient of diffusion that describes the efficiency of diffusion. Experimental results [*Rutter*, 1976; *Gratier and Guiguet*, 1986; *Schutjens*, 1991; *Spiers and Brzesowsky*, 1993; *Hickman and Evans*, 1995] have shown that this product is between 10^{-18} and 10^{-21} m³/s. In experiments with an indentation of halite on calcite surfaces, this product has been estimated to be around 10^{-20} m²/s at 30°C [*Gratier*, 1993a, 1993b]. This value is in good agreement with experimental results on aggregates.

[19] The diffusion coefficient depend also on the water film thickness. Thin films (a few molecular layers of water) will have major affinity to the mineral surfaces and may behave more like solids than free water [*Rutter*, 1976; *Israelachvili*, 1986]. Because of the lack of knowledge about this process, we will consider, as a first approximation, that the coefficient of diffusion is constant in the water film.

3. Rate of Pressure Solution

[20] In the following we will analyze the pressure solution processes for a geometrically simple model. In a closed domain, spherical grains are in contact, surrounded by a pore fluid. The contact surface is circular with a radius R_{cont} (R_{cont} is equal to R_x, R_y, and R_z in Figure 2). In geological systems, the contact radius can vary from 10^{-6} m in siltstones to 10^{-2} m for conglomerates. For each step (dissolution, diffusion, precipitation), one can determine a rate of deformation of the contact surface: a rate for dissolution, a rate for diffusion, and a rate for precipitation. The slowest rate gives the overall rate of the deformation process if the deformation proceeds in a sequence of instantaneous steady state and when the system is closed with respect to long range transport of dissolved solid [*Raj*, 1982; *Caron et al.*, 1987; *Mullis*, 1993; *Shimizu*, 1995]. In an open system we can define three dimensionless numbers which quantifies under which conditions dissolution, precipitation, or contact diffusion acts as the rate-limiting process (E. Gundersen et al., Pressure solution in sandstone, rate-limiting processes and the effect of clays, submitted to *Journal of the Geological Society (London)*, 2001, hereinafter referred to as Gundersen et al., submitted manuscript, 2001).

3.1. Diffusion at the Contact

[21] The flux of material that is expelled by diffusion from the grain contacts, J_{diff} (mol/m² s), can be described as

$$J_{diff} = \frac{D_{cont}(c_{cont} - c_{pore})}{R_{cont}} \qquad (2)$$

where $(c_{cont} - c_{pore})/R_{cont}$ (mol/m³ m) is the gradient of concentration between the contact and the pore, D_{cont} (m²/s) is the coefficient of diffusion, and the effective normal stress (and hence c_{cont}) is assumed constant within the contact. *Weyl* [1959] and *Rutter* [1976] have solved the more complicated case where the stress profile along the contact is not flat and the diffusion becomes two-dimensional. The calculated gradient of concentration is modified by a factor of 2 to 3. For simplicity, we will not consider this 2-D effect within the grain contacts.

3.2. Dissolution and Precipitation Steps

[22] The rate of dissolution at the surface of contact J_{diss} (mol/m² s) is given by

$$J_{diss} = k_{diss}\left(1 - \frac{c_{cont}}{K_{cont}}\right) \qquad (3)$$

where k_{diss} is the kinetic coefficient for dissolution (mol/m² s), c_{cont} refers to the concentration inside the water film (mol/m³), and K_{cont} is the equilibrium solubility inside the water film. Note that this rate has the same units as the diffusion flux. The rates of dissolution and precipitation are calculated with an equation based on the transition state theory [*Lasaga*, 1998] which describes how the mass of a reactant, m_{rxn}, evolves with time:

$$\left(\frac{\partial m_{rxn}}{\partial t}\right)_z = k_r s_r a\left[1 - \exp\left(-\frac{A_r}{RT}\right)\right] \qquad (4)$$

where k_r and s_r are the rate constant and mineral surface area, a is the activity of the dissolved specie, and A_r stands for the chemical affinity for the dissolution/precipitation reaction. The affinity is given by

$$A_r = RT \ln\left(\frac{Q}{K}\right) \qquad (5)$$

where Q is the reaction quotient and K the equilibrium constant for dissolution. Such equations accurately describe dissolution from far to near equilibrium conditions [*Lasaga*, 1998].

[23] For the precipitation step (step 3 in Figure 1), the flux of deposited matter on the free surface inside the pore J_{prec} (mol/m² s) is given by

$$J_{prec} = k_{prec}\left(1 - \frac{c_{pore}}{K_{pore}}\right) \qquad (6)$$

where c_{pore} is the concentration inside the pore fluid, K_{pore} is the equilibrium solubility in the pore fluid, and k_{prec} the kinetic coefficient (mol/m² s). By convention, fluxes of dissolution are positive while fluxes of precipitation are negative.

[24] In geological systems, the fluid composition can vary and modify both the kinetics of reaction and the mineral solubility. For example, at basic pH the kinetics of quartz dissolution/precipitation is faster and the solubility higher

than at acidic or neutral ones [*Dove*, 1994] and the rates of deformation can be speeded up by several orders of magnitude. The reaction kinetics do exert a strong control on the rate at which compaction and cementation occur. The choice of the kinetics constant for quartz dissolution and precipitation is a major issue when simulating quartz cementation. The kinetic constant for dissolution/precipitation reactions has been estimated under laboratory conditions for quartz [*Dove*, 1994] and calcite [*Plummer et al.*, 1978; *Plummer and Busenberg*, 1982]. *Walderhaug* [1996] has estimated the kinetics of quartz precipitation from geological observations in North Sea sandstones and found rates several orders of magnitude smaller than what is measured under laboratory conditions. Such difference between geochemical reaction rates measured in laboratory and natural systems is a well-known problem in geologic systems [*Malmstrom et al.*, 2000]. The rates deduced from observations in natural systems might be more relevant during modeling of diagenetic processes (e.g., timescales of several million years). Because of the lack of knowledge of such rates under natural conditions, we will vary the rate of precipitation (equation (6)) between the two end-members found in the literature [*Dove*, 1994; *Walderhaug*, 1996].

3.3. Diffusive Transport of Solutes in the Pore Space

[25] So far, we have only considered dissolution at the grain contacts and local precipitation in the pore adjacent to that contact. If solutes are allowed to migrate between pores, we need to include a concentration driven global diffusion in the model. Spatially variable compaction is often observed where highly compacted bands of material alternate with bands of lower deformation, indicating transport of solute in the pore space. This is the case for stylolites where planes of dissolution are oriented perpendicular to the principal stress. The mean distance between stylolites varies depending on the rock composition; 0.1 to 2 cm in sandstones and 1 to 10 cm in limestones [*Merino*, 1990]. The occurrence of stylolites alternating in a regular pattern is still debated [*Merino et al.*, 1983; *Railsback*, 1998]. During stylolitization, there is a transport of solutes over distances greater than a single grain [*Oelkers et al.*, 2000]. The minimum scale of closed system behavior is half stylolite spacing; in carbonate rocks, this distance is usually two orders of magnitude larger than the grain scale. For some quartz arenites and quartzites, microstylolites are only one grain-length apart and come in swarms of 10, 20, or even more. The appropriate scale then becomes the distance between swarms (not that between microstylolites) and is, then, much larger than the grain scale. Transport of solute, here by diffusion, in the pore space indicate how "open" the system is. Advective transport of solute in a moving solvent is not considered in this contribution, but it will be a natural extension of the model.

[26] In order to combine global diffusive mass transport in the pore network with local deformation by pressure solution we solve a set of highly coupled nonlinear equations. The equations are derived by a global mass balance of the solute phase in the pore volume and a local mass balance at each grain contact. Those equations are then coupled to equations which express grain-contact deformation and the evolution of rock texture for grains having a truncated spherical geometry (see Figure 2). All the param-

eters used in the following equations and their units are given in Table 1.

[27] The mass balance for the solute phase in the pore volume is given as

$$\phi \frac{\partial c_{\text{pore}}}{\partial t} = D_{\text{pore}} \nabla^2 c_{\text{pore}} + \frac{1}{L_x L_y L_z} \left[\frac{\partial m_{prec}}{\partial t} + 2 \sum_{i=1}^{3} \frac{\partial m_{diff,i}}{\partial t} \right] \quad (7)$$

where c_{pore} is the concentration of solute in the pore fluid, ϕ is the porosity, and the lengths L_x, L_y, and L_z are defined in Figure 2. The first term on the right side in equation (7) describes the diffusive transport of solutes in the pore space via Fick's law. The coefficient of diffusion D_{pore}, in the pore fluid is assumed to follow an Arrhenius law [*Nakashima*, 1995]. The driving force for this transport is a concentration gradient due variations in stress concentrations at grain contacts between domains with different grain sizes, all other contributions to chemical potential gradients driving diffusive mass transfer are neglected (see equation (1)). In our model we assume a constant coefficient of diffusion. A further refinement of this model is to take into account some porosity-dependent tortuosity factor in the diffusion coefficient. However, numerical tests indicate that such tortuosity would not significantly modify the results of the simulations. The decrease in the length of the diffusion path is taken into account for porosity reduction due to compaction.

[28] The next term in equation (7), which represents changes in solute mass due to precipitation in the pores, is given as

$$\frac{\partial m_{prec}}{\partial t} = k_{prec} A_{\text{pore}} \left(1 - \frac{c_{\text{pore}}}{K_{\text{pore}}} \right) \quad (8)$$

where k_{prec} is the kinetic coefficient of precipitation, K_{pore} is the equilibrium concentration of solute in the pore fluid and A_{pore} is the grain surface in contact with the pore fluid. Notice that as the spheres changes during simulation, $A_{\text{pore}} = g(L_f, L_x, L_y, L_z)$ varies correspondingly.

[29] The last term in equation (7) describes the solute mass change in the pore volume due to diffusion from the grain contact into the pore volume.

$$\frac{\partial m_{diff,i}}{\partial t} = 2\pi \frac{\Delta_i}{2} D_{cont} \left(c_{cont,i} - c_{\text{pore}} \right) \quad (9)$$

where $c_{cont,i}$ is the concentration of solute in a grain contact in the i-direction. Note, that in equation (7) this term is summarized over all the six contact areas of a truncated spherical grain (see Figure 2). The thickness of the water film at the grain contacts, Δ_i is divided by two since it is shared between two contact surfaces. The coefficient of diffusion inside the water film D_{cont} follows an Arrhenius law, see *Gratier and Guiguet* [1986].

[30] The global diffusion equation (7) is then coupled to six equations which represent the local mass balance for each contact on the sphere.

$$\frac{\partial c_{cont,i}}{\partial t} = \frac{1}{\pi R_{cont,i}^2 \frac{\Delta_i}{2}} \left[\frac{\partial m_{diss,i}}{\partial t} - \frac{\partial m_{diff,i}}{\partial t} \right]. \quad (10)$$
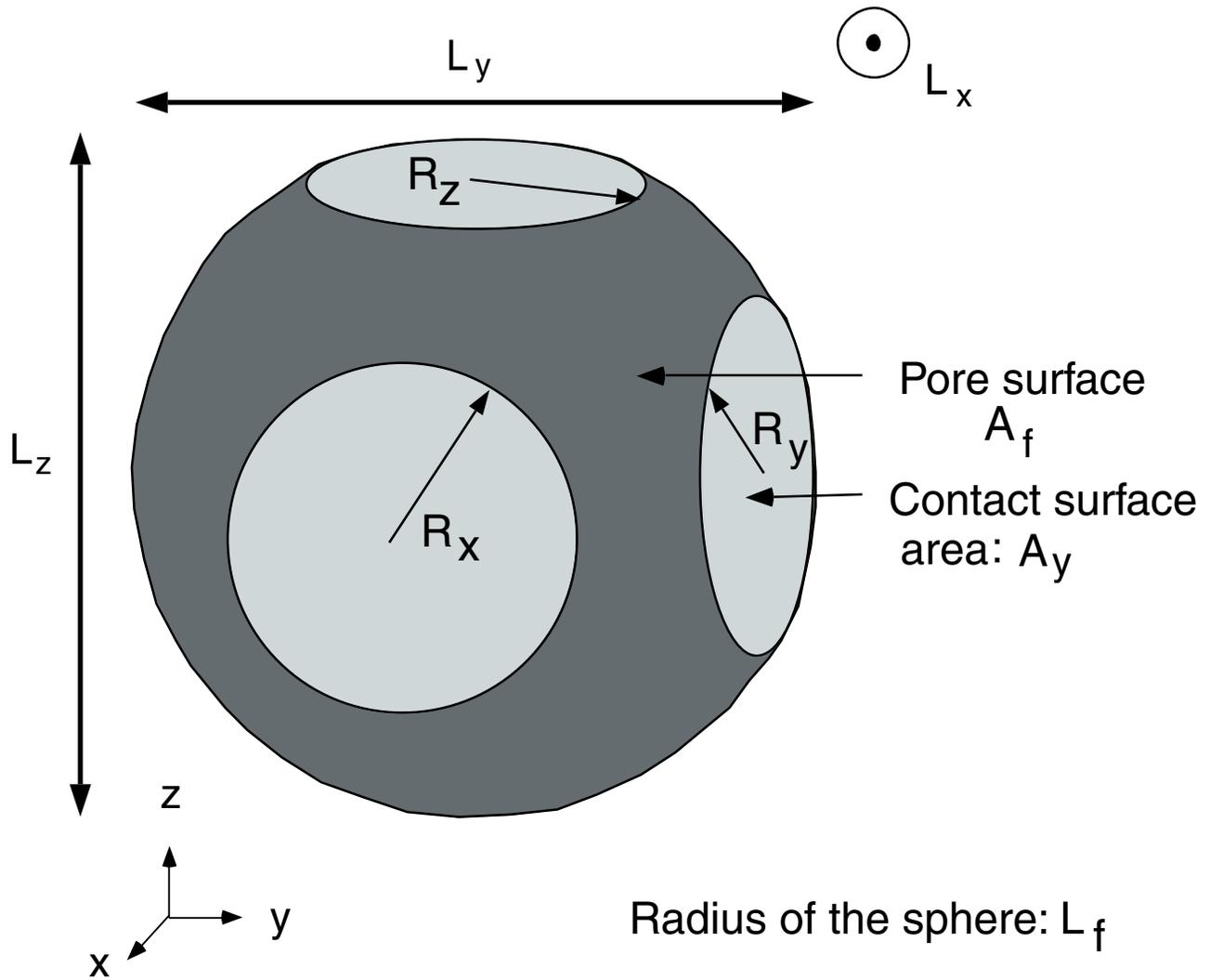
Figure 2. Schematic representation of a single grain for which the surface is divided into contacts with other grains (light areas) and free faces in contact with the pore fluid (dark area). Each grain has six neighbors, arranged in a cubic packing.

Here, the index i represents the space dimensions, $i = x, y, z$, and $R_{cont,i}$ is the radius of the contact surface in the i direction, which is a function of the spherical lengths. The second term on the right side in equation (10) represents dissolution of solute into the grain-boundary film and is given as

$$\frac{\partial m_{diss,i}}{\partial t} = k_{diss} A_{cont,i} \left(1 - \frac{c_{cont,i}}{K_{cont,i}} \right) \qquad (11)$$

where $A_{cont,i}$ is the surface area of the grain-film-grain contact in the i direction, k_{diss} is the kinetic coefficient of dissolution, and $K_{cont,i}$ is the equilibrium concentration of solute in a contact in the i direction. The last term in equation (10) represents the local mass transport out of the contact and into the pore space by diffusion, as given by equation (9). Note that the part of the sphere which is dissolved is approximated as a cylinder; thus, this analysis is most valid for small strains.

[31] As dissolution, diffusion in the contact, and precipitation are fully coupled processes (through equations (8), (9), and (11)) there is not any assumption on which step is the slowest. Depending on the thermodynamic parameters the system finds automatically the step which controls the whole process.

[32] The grain shape evolution is given by the four equations

$$\frac{dL_i}{dt} = -2k_{diss} \bar{V}_s \left(1 - \frac{c_{cont,i}}{K_{cont,i}} \right) \qquad (12)$$

$$\frac{dL_f}{dt} = -k_{prec} \bar{V}_s \left(1 - \frac{c_{pore}}{K_{pore}} \right) \qquad (13)$$

where again the index i is given as $i = x, y, z$ and $\bar{V}_s$ is the molar volume of the dissolving mineral.

[33] The simulation domain is a 2-D squared rock sample located several kilometers below the surface where it is exposed to stress and a temperature field. We neglect shear

Table 1. Symbols and Units Used in Equations (1)−(16)

Parameter	Description	Unit
$A_{cont,i}$, $i = x, y, z$	contact area in the i-direction	m^2
A_{pore}	pore surface area	m^2
$c_{cont,i}$, $i = x, y, z$	concentration in a grain contact in the i-direction	mol/m^3
c_{pore}	concentration in the pore fluid	mol/m^3
D_{cont}	diffusion constant in the grain contact	m^2/s
D_{pore}	diffusion constant in the pore	m^2/s
J_{diff}	flux of matter transported by diffusion out of the contact	mol/(m^2 s)
J_{diss}	flux of dissolution of the contact surface	mol/(m^2 s)
J_{prec}	flux of precipitation on the pore surface	mol/(m^2 s)
k_{diss}	kinetic coefficient of dissolution	mol/(m^2 s)
k_{prec}	kinetic coefficient of precipitation	mol/(m^2 s)
K_{cont}	equilibrium constant in the contact	mol/m^3 for silica
K_{pore}	equilibrium constant in the pore	mol/m^3 for silica
L_i, $i = x, y, z$	length of the truncated sphere in the i-direction	m
L_f	radius of the spherical grain	m
P_f	pore fluid pressure	Pa
$R_{cont,i}$, $i = x, y, z$	radius of a grain contact in the i-direction	Pa
$\bar{V}_s$	molar volume of the dissolving mineral	m^3/mol
Δ_i	thickness of the water film in the contacts, in the i-direction	m
ϕ	porosity	
σ_{ni}, $i = x, y, z$	normal stress component in the i-direction	Pa
σ_{ni}, $i = x, y, z$	normal stress to a grain surface in the i-direction	Pa

stresses and relate the in-situ stress component σ_i to the local normal stress at the grain contacts σ_{ni} by the three equations

$$\sigma_{n_x} = \sigma_x \frac{L_y L_z}{A_x} \qquad (14)$$

$$\sigma_{n_y} = \sigma_y \frac{L_x L_z}{A_y} \qquad (15)$$

$$\sigma_{n_z} = \sigma_z \frac{L_x L_y}{A_z}. \qquad (16)$$

Assuming that the applied tectonic stresses are kept constant, it is seen that the contact area A_i increases and the local stress normal to this grain contact decreases as the grain becomes more and more truncated. Therefore, under conditions of constant applied stress, the driving force for pressure solution diminishes with time. In order to conserve the mass inside the domain, no flux boundary conditions have been applied for the concentration of dissolved material.

[34] Finally the model includes several algebraic functions to calculate textural parameters (e.g., the length L_x and the radius R_x) for each grain, and the porosity ϕ as defined by *Renard et al.* [1999]. These relationships arise from the textural model of truncated spheres ordered in a centered cubic network

4. Numerical Models and Boundary Conditions

[35] The differential equations (7)−(13) are solved using a Galerkin finite element method with linear basis functions on the spatial domain and a Crank-Nicolson scheme in the time domain. The numerical schemes were programmed in C++ and make use of the numerical library Diffpack [*Langtangen*, 1999].

[36] The space domain is taken to be a two-dimensional rock sample, modeled as a cubic packing of truncated spheres (Figure 3). Each element in the numeric grid consists of a fixed number of equally sized spheres. The

heterogeneity of the rock sample is then simulated by varying sphere size among the elements.

[37] Two of the boundaries are fixed as stiff walls on which the side of the simulated domain can slip. A no-flux condition for the solute phase was imposed for these two boundaries. The other two boundaries are free and deform during the simulation. Here different types of boundary conditions have been tested. In most of the examples no flux conditions were imposed; however, boundary conditions open for flow were also tested in order to quantify transport of solute across the boundaries. It turned out that the flux through the boundary is small and hardly contributes to the global mass balance in these simulations. As this is a 2-D model, no strain and mass flux were allowed in the y direction (see Figure 3). The stress at the boundaries is constant during a simulations, usually fixed as $\sigma_x = \sigma_y = 60$ MPa and $\sigma_z = 66$ MPa. However, other values have also been used.

[38] On an adaptive grid, the nodes move in each time step in order to simulate the deformation. Moreover, the size of each element is reduced after each time step by the same amount as the lengths (L_x, L_z) of the sphere. The total reduction in element size is then given as the product of the length of the truncated spheres and the number of spheres in the element. When no solute mass flux is permitted across the freely deforming boundaries, the volume lost in the grid during the simulation equals the loss of porosity.

[39] For simplicity we have assumed no gradients in temperature or fluid pressure due to gravity or other causes within the simulation domain. This assumption is valid because we model processes at the scale of only a few meters. The program was extensively tested for numerical stability. In all the simulations we tested the total mass of solid was conserved to within ±0−2%.

5. Simulation of Coupled Pressure Solution and Transport by Diffusion

[40] In most of the simulations, the 2-D domain is a 20 × 20 cm rock situated at a depth of 3 km, and with a thickness
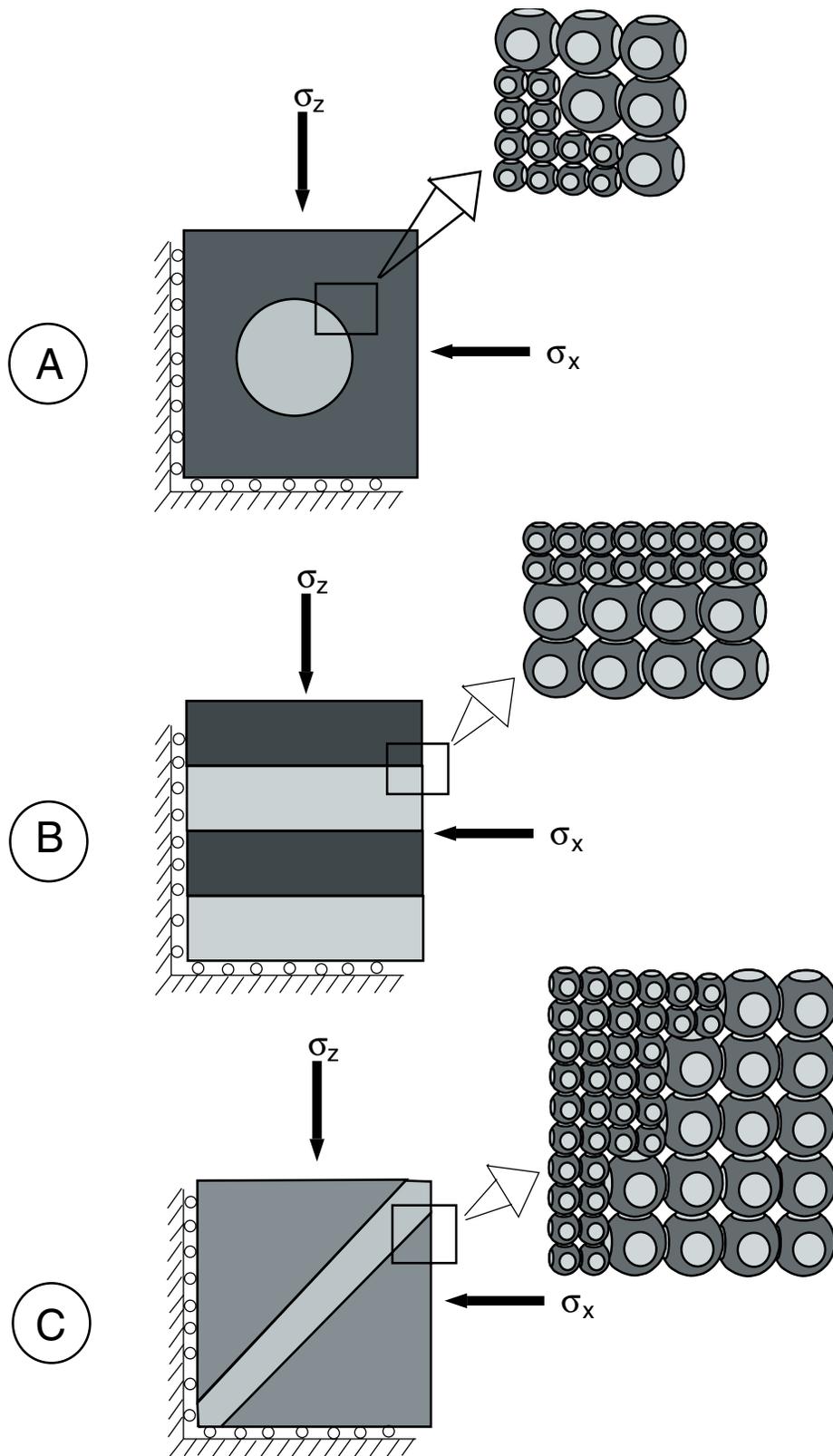
Figure 3. Domains where coupled pressure solution creep and local diffusive mass transport are simulated. Each element in the numerical grid contains a given number of grains with the same size. The domain is two-dimensional (x and z directions) and has a thickness of one layer of grains in the y direction. The grain size and porosity can vary between the elements. Here are presented the three geometries simulated. In case (A) the grains size heterogeneity is located in a circular region in the center of the grid, case (B) corresponds to layers of alternating smaller and larger grain sizes and finally, in case (C) the small grains are located in a layer between coarser grained particles and are meant to represents fault gouge.

of one layer of grains. The rock sample compacts as porosity is lost during the simulation. The temperature in the domain is constant at 375°Kelvin. Pressure solution is the only compaction process included in the model. Moreover, we assume that other processes, such as cataclasis with or without accompanying subcritical crack growth, do not occur. In all the simulations the pore fluid pressure was constant, P_{pore} = 30 MPa. The horizontal stresses, $\sigma_x = \sigma_y$ = 60 MPa and the vertical stress, σ_z = 66 MPa. The initial radius of the spheres, L_f varies in the different simulations. The other lengths, describing the truncated spheres, L_x, L_y, and L_z are given as $2 \cdot 0.90 \cdot L_f$. This corresponds to an initial porosity of 31%.

[41] The simulations last until the porosity in the whole simulation domain is less than 3%. We assume that when the porosity is below 5% in an element, a percolation threshold for that element is reached [Feder, 1988]. In these elements transport with other elements will terminate and pressure solution will continue locally inside this element, as a closed system. Moreover, if the percolation threshold is reached in an element, the second term in equation (7) is set to zero for that element.

[42] The simulation domain is divided into 60 × 60 elements. The time step is adjusted such that the increment of the deformation is less than 0.1% between each time increment. Therefore, the time step automatically adapts in the regions with the most rapid deformation.

[43] In the following simulations we have chosen to primarily use the reaction kinetics data derived in laboratory experiments [Dove, 1994], for which the activation energies as a function of fluid salinity and pressure are known. We will also study the case where the kinetics of quartz cementation is reduced in accord with observations in natural systems [e.g., Walderhaug, 1996] to see how this modifies the rate of compaction.

5.1. Circular Porosity Heterogeneity

[44] In the first simulation the domain contains two areas of different grain sizes to model the formation of nodules in sedimentary rocks. Some of these patterns are believed to correspond to the amplification of an initial porosity or other heterogeneity [Bjørkum and Walderhaug, 1990], such as epigenetic concretions that form during late diagenesis after consolidation of the enclosing sediment [Berner, 1968; Raiswell, 1971]. To simulate their formation, one domain is shaped as a circle (the concretion), while the other is the surroundings (see Figure 3a). The small grain size is given as L_f = 90 micron while the large one is equal to L_f = 130 micron. Within each domain the grain size is homogeneous. Because of this initial grain size difference, the two domains compact with different rates and the domain with the small grains exports some silica to the surroundings (see Figure 4).

[45] When the small grains are inside the concretion, the concretion compacts as a soft object compared to the matrix (see Figures 4a, 4b and 4c). In the opposite case the concretion behaves as a hard object resistant to compaction (Figures 4d, 4e, and 4f). In both cases, the simulations indicate a local transport of silica from the regions of small grains to the regions where grains are larger such that the concretion containing the large grains grow while the ones containing the small grains shrinks. The result is the development of a gradient of porosity over time. These

simulations constrain the timescales for the development of concretions only if there are no other processes such as nucleation threshold or fluid flow occurring. In the latter case, the simulations only provide maximum timescales for concretion growth as advective fluid flow would accelerate solute mass transfer.

[46] When many concretions nucleate in close proximity to one another (e.g., in the same sedimentary layer), they may compete with one another during solute import or export. The result is that the region between the two concretions can become overcemented, if it contains large grains, or loose additional solute mass if it contains small grains (see Figure 5). The effect of this interaction becomes less important as the distance between concretions increases such that the two concretions are located outside the diffusive transport distance of one another. The transport distance depends on the rate control of the whole process (Gundersen et al., submitted manuscript, 2001). Typical observations in sandstones with calcite cement indicate that such effects occur for concretion spacings less than several centimeters and disappear above one decimeter [Bjørkum and Walderhaug, 1990]. Our simulations indicate a critical length scale for this process of close to 5 cm in pure sandstones.
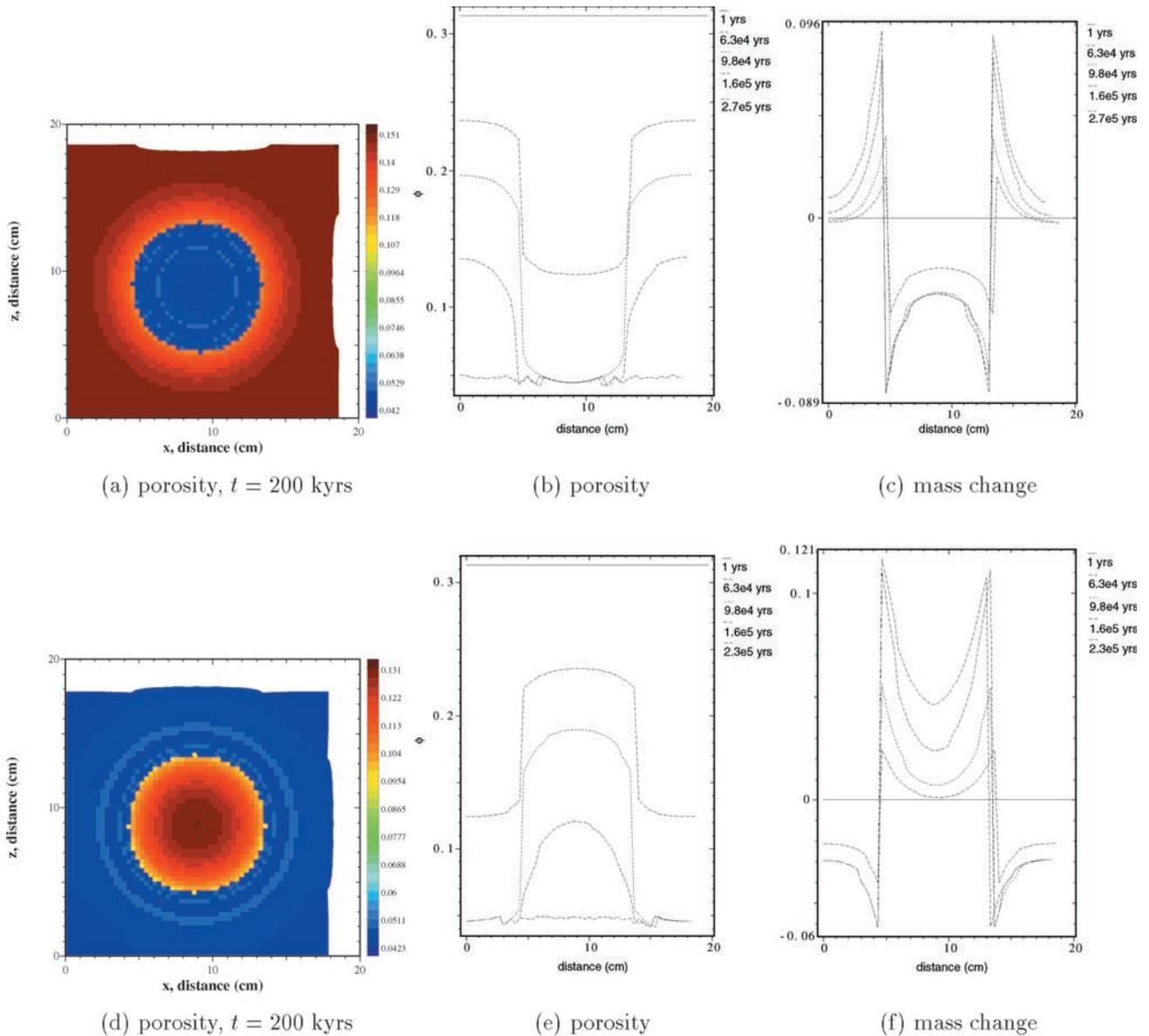
5.2. Diagenetic Layering in Sedimentary Rocks

[47] To simulate the formation of diagenetic layering, the domain is divided into five layers (Figure 6). In each layer the initial grain size is specified as a uniform random distribution between a minimum and a maximum value. In three of the layers L_f is uniformly distributed between minimum and maximum values of 115 and 130 micron, respectively. In the following we use the abbreviation $L_f \sim$ uniform (115, 130) micron when referring to uniform random distributions. In the last two layers $L_f \sim$ uniform (100, 115) micron. The other textural parameters are $L_x = L_y = L_z = 2 \cdot 0.95 \cdot L_f$ which leads to an initial uniform porosity of 31% throughout the whole domain. In all of the results presented here the normal stress at the external boundaries, and the temperature have been kept constant.

[48] Figure 6 shows how porosity (a–c), accumulated mass transported by diffusion (d–f) and concentration of silica (g–i) varies during the simulation. There are two different length scales for diffusive mass transfer in this example. Those resulting form the macroscopic layers and those associated with the random scatter in grain size within the broadly specified range of grain sizes for each layer. The latter results in a highly localized diffusive mass transfer on the grain scale.

[49] In Figure 6a only small porosity variations occur after 3.2×10^3 years. In each layer the porosity varies within (1–2)% which is essentially caused by the initial random scatter in grain size. At longer wavelengths, we see that the two layers containing the smallest grains have compacted more than the layers with larger grains. After 8.0×10^4 years, Figure 6b shows a larger variation in the porosity in each layer and larger differences between the layer with small and large grains.

[50] The smallest porosity values are found in the two layers containing the small grains. Here, the variation in the porosity is about 2% between the maximum and minimum value. This small variation is mainly caused by the initial random scatter in the grain size, and the porosity

(a) porosity, $t = 200$ kyrs

(b) porosity

(c) mass change

(d) porosity, $t = 200$ kyrs
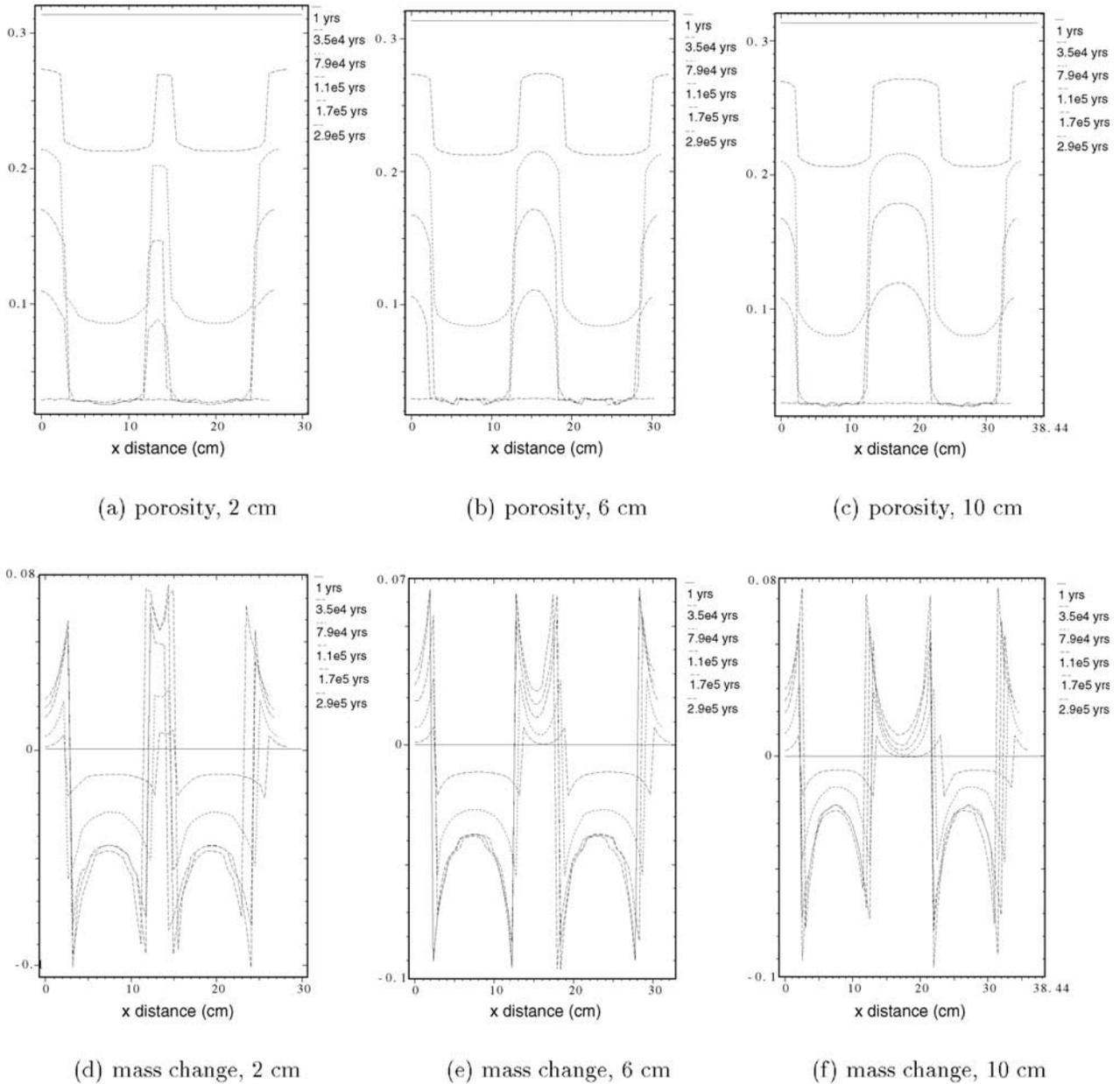
(e) porosity

(f) mass change

Figure 4. Compaction and porosity variations around a concretion with a different grain size than its surroundings. Axes are in cm. The temperature and stress conditions are similar to that at 3 km depth. The mineralogy is pure quartz with initial grain size 90 microns in the concretion and 130 microns in the surroundings (a, b, c), and 130 microns in the concretion and 90 microns in the matrix (d, e, f). Moreover, in the top three plots, small grains are placed inside the circle while the large grains are in the surroundings. This is the opposite for the three bottom cases. Figures (a) and (d) show the porosity distribution after a given time of compaction. The curves in plot (b) and (c) indicate the porosity evolution along the cross section line $x = 10$ cm. Plots (c) and (f) represent the mass of silica transported by diffusion in a section passing through the center of the concretion. The mass diffused corresponds to the variation of mass (%) of an element compared to its initial mass before deformation. Clearly, silica is exported in regions of small grains size to regions of coarser grains.

loss is due to grain indentation. Mass is lost from these layers.

[51] In the three layers containing the largest grains the porosity variation is (4–5)% between the smallest and the largest value. In these layers we see that the area with the smallest porosities are located close to the boarder of the small grain layers. Here porosity is lost both due to grain indentation as well a cementation, where the cement con-

sists of mass transported from the small grain layers. The largest porosity values are located outside of the diffusive transport distance of the small grain layers. Here, porosity is lost only by grain indentation.
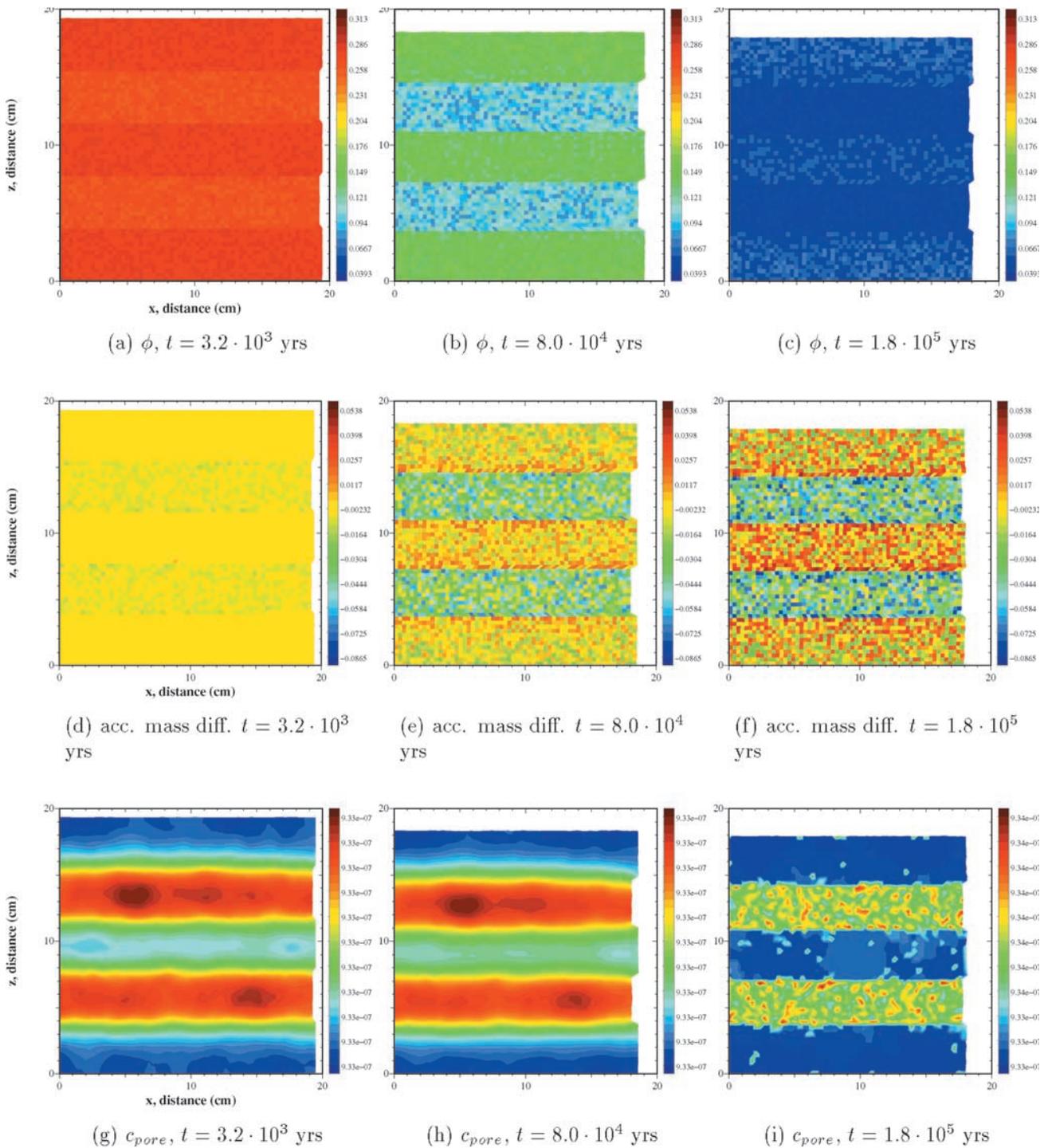
[52] After 1.8×10^5 years (Figure 6c) the compaction process is almost finished and the porosity distribution is now dominated by short-wavelength variations in compaction due to the initial random distribution of grain sizes.

(a) porosity, 2 cm   (b) porosity, 6 cm   (c) porosity, 10 cm

(d) mass change, 2 cm   (e) mass change, 6 cm   (f) mass change, 10 cm

Figure 5. Compaction and porosity variations in the case of two concretions, represented as circles with grain size $L_f = 90$ micron whereas the grain size in the surroundings is $L_f = 130$ micron. The curves in plots (a), (b) and (c) indicate the porosity evolution along a line passing through the center of the two concretions. Plots (d), (e), and (f) represent the mass of silica transported by diffusion in a section passing through the two centers of the concretions. The distance between the concretions is 2 cm in plots (a) and (d), 6 cm in plots (b) and (e), and 10 cm in plots (c) and (f). As this distance increases, the interaction between the concretions becomes smaller.

[53] The next three plots (Figures 6d–6f) show the accumulated diffusive mass transport over time, depicted as the mass of solid in an element at time t minus its initial mass in time t_0, and normalized to the mass at time t_0. The unit are % of initial mass transported. A positive value indicates a cemented area which has received mass, whereas a negative value represents an element which looses mass during compaction. Plots (e)–(g) clearly indicate how fare mass is transported from the small grain layers and into the large grain layers.

[54] The last three plots (Figures 6g–6i) show the concentration of dissolved silica in the pore fluid over time. Plot (g) and (h) show a pronounced decrease in the concentration gradient of silica over time. In plot (i) the percolation threshold has been reached. Then variations of dissolved silica are only due to the initial random grid size distribution. In the simulation shown here the diffusion coefficient, D_p is constant as long at the porosity is larger than the percolation threshold, and $D_p = 0$ below this threshold. Other simulations (not shown wherein) where D_p decreases

(a) ϕ, $t = 3.2 \cdot 10^3$ yrs

(b) ϕ, $t = 8.0 \cdot 10^4$ yrs

(c) ϕ, $t = 1.8 \cdot 10^5$ yrs

(d) acc. mass diff. $t = 3.2 \cdot 10^3$ yrs

(e) acc. mass diff. $t = 8.0 \cdot 10^4$ yrs

(f) acc. mass diff. $t = 1.8 \cdot 10^5$ yrs

(g) c_{pore}, $t = 3.2 \cdot 10^3$ yrs

(h) c_{pore}, $t = 8.0 \cdot 10^4$ yrs

(i) c_{pore}, $t = 1.8 \cdot 10^5$ yrs

Figure 6. Amplification of porosity contrast during chemical compaction of a sandstone. The initial size of the domain is 20×20 cm with a 60×60 elements grid. Moreover, the initial state corresponds to layers with the same porosity but with different random distributed grain size. In layers 1, 3, and 5: $L_f \sim$ uniform (115, 130) micron, and for layers 2 and 4: $L_f \sim$ uniform (100, 115) micron. The other textural parameters are $L_x = L_y = L_z = 2 \cdot 0.95 \cdot L_f$. This leads to an initial porosity of 31%. The stress and temperature conditions are those at 3 km depth. Plots (a), (b), and (c) show the porosity evolution while plot (d), (e), and (f) represent the accumulated mass transported by diffusion in the region of larger grains. The last three plots (g), (h), and (i) show the concentration of silica.

(a) porosity evolution   (b) mass diffused
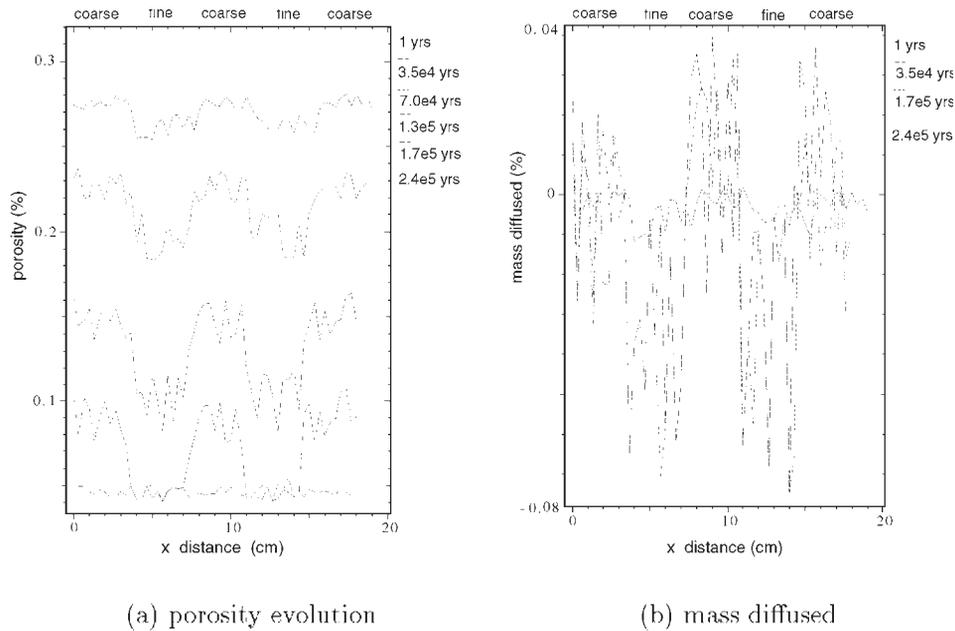
Figure 7. Cross sections perpendicular to the layers of Figure 6, representing the porosity and the mass evolution along the line $x = 10$ cm at various elapsed times t. (a) The process of compaction amplifies the porosity contrast between the layer. The irregularities in each layer reflects the initial randomly distributed grain sizes. (b) Mass transported by diffusion between the layers. Layers with larger grains show about a 4% increase in mass due to transport from layers with smaller grains.

linearly with porosity lead to only minor changes in the porosity as well as the accumulated diffusive transport.

[55] The simulations show that compaction, as measured by porosity loss, occurs everywhere but is faster in the layers with smaller grains. Again, silica is exported from layers of small grain size to layers with larger grains. The coarsest grained layers become cemented and are characterized by quartz overgrowth. Here the overgrowth is more important for the porosity reduction than grain indentation and compaction due to pressure solution.

[56] Figure 7 shows several cross-sections taken along a line perpendicular to the layers in Figure 6. Each curve is taken at a different time step during the simulation and shows the evolution of porosity (Figure 7a) and element mass (Figure 7b). The porosity differences between the two layers increase, until the percolation threshold is reached at a porosity of about 5%, after which the porosity equalizes. The mass exported or imported by the fine- and coarse-grained layers, respectively, also increases with time, indicating that the transport is active during the whole compaction process up until the percolation threshold (see Figure 7). The shorter-wavelength variations in porosity and mass change in each layer arise from the initial random variations in grain size.

[57] Additional simulations in which the initial contrast in grain size is allowed to vary show that there is a characteristic timescale for the compaction of each layer that depends on the grain-size contrast (Figure 8). The porosity contrast between the layers increases with time at the beginning of compaction until the layers with small grains reach a percolation threshold and compact as individual grains. The compaction process stop when the porosity is less than 3%. At this stage, the layers with larger grains continue to compact and the porosity contrast starts to decrease. For a large initial grain size difference between the layers, the porosity difference becomes greater and lasts for a longer time until the whole domain has reached 3% porosity (Figure 8).

[58] The kinetics of quartz dissolution/precipitation measured in the laboratory [*Dove*, 1994] or estimated from geological observations [*Walderhaug*, 1996] differ by several orders of magnitude. The simulations of Figure 9 are performed with quartz precipitation kinetics varying between these two end-members. When precipitation is fast relative to diffusion through the pore fluid or grain-boundary film, the kinetics of quartz compaction are diffusion rate-limited and the time at which the porosity of the rock reaches 3% does not depend on the rate of precipitation (i.e., $k_{prec} \geq 10^{-17}$ to 10^{-15} mol cm^2/s in Figure 9). Instead, compaction is controlled by the rate of diffusion along grain contacts. When the rate of precipitation becomes less than the diffusion rate the compaction time-scale depends on the rate of precipitation and the process becomes surface-reaction controlled. The transition between diffusion-controlled and precipitation-controlled compaction varies with burial depth and grain size. Figure 9 show only the burial depth dependence, the grain size are equal to the ones used in Figure 8.

5.3. Cementation Around a Fracture Containing a Gouge

[59] In this section we examine the porosity evolution within and around a fracture. The simulation domain (Figure 3c) contains a closed fracture filled with a gouge with smaller grains. The grain sizes are the following: in the gouge $L_f \sim$ uniform (40, 60) micron, on the left wall of the
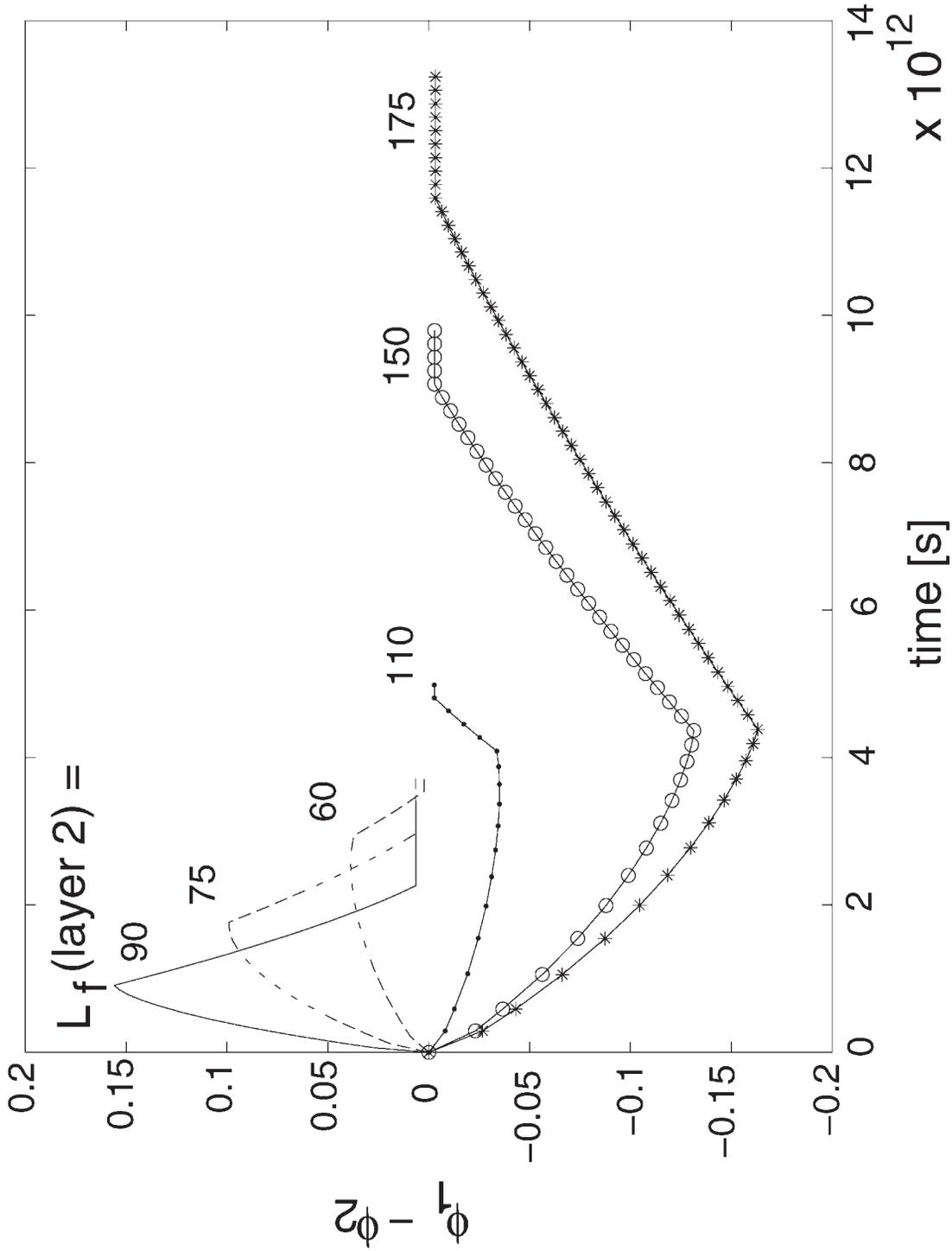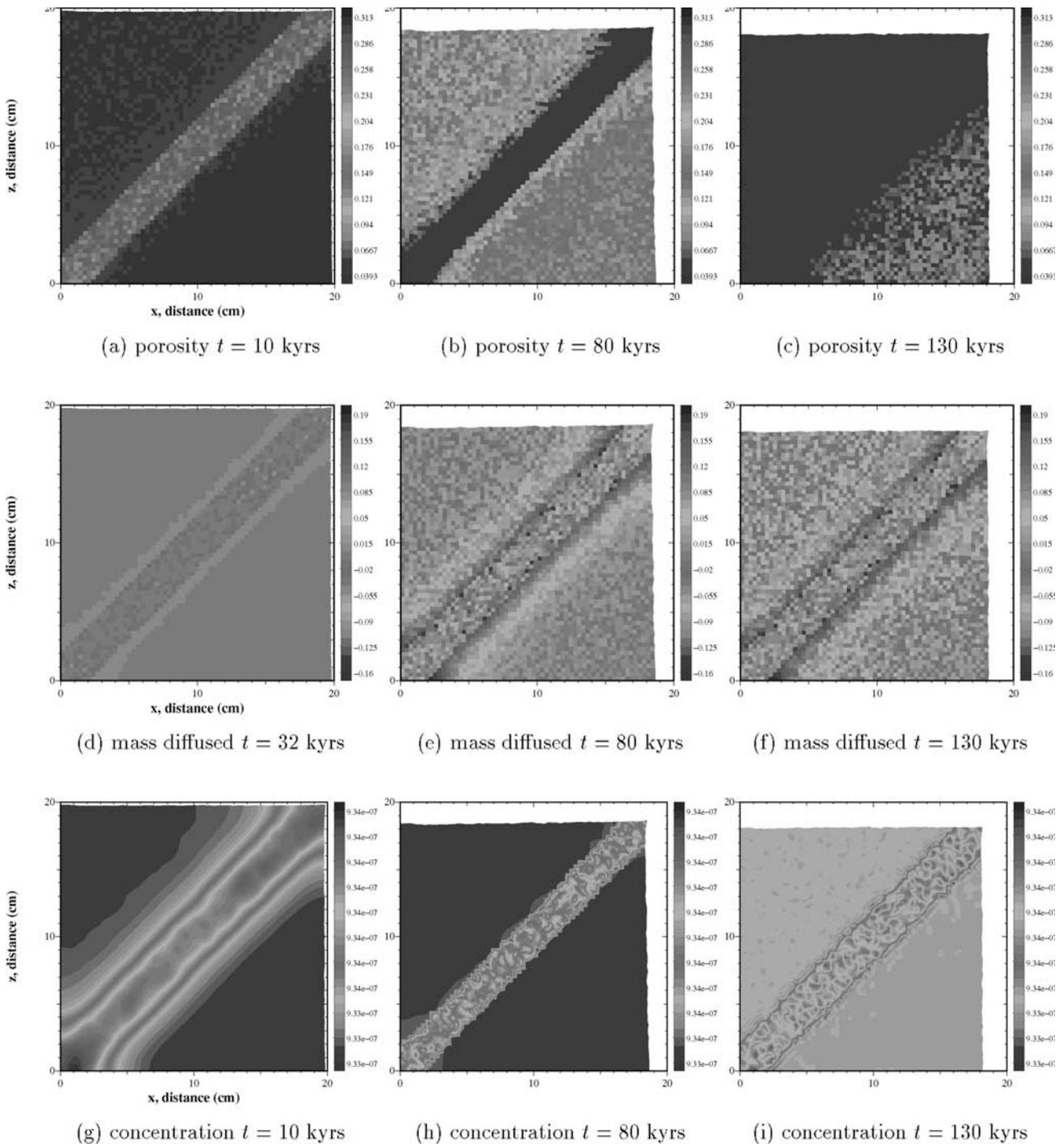
Figure 8. Porosity contrast ($\phi_1 - \phi_2$) between two layers of different grain size as a function of time. In all the curves, initial grain size in layer 1 is given as $L_f = 100$ micron. For layer 2 the grain size varies between 60 and 175 microns for the different curves. For all simulations the porosity contrast initially increases as the layers with smaller grain size compact faster. Then, as these layers have reached 5% porosity, the porosity contrast decreases because only layers with coarser grains continue to compact.
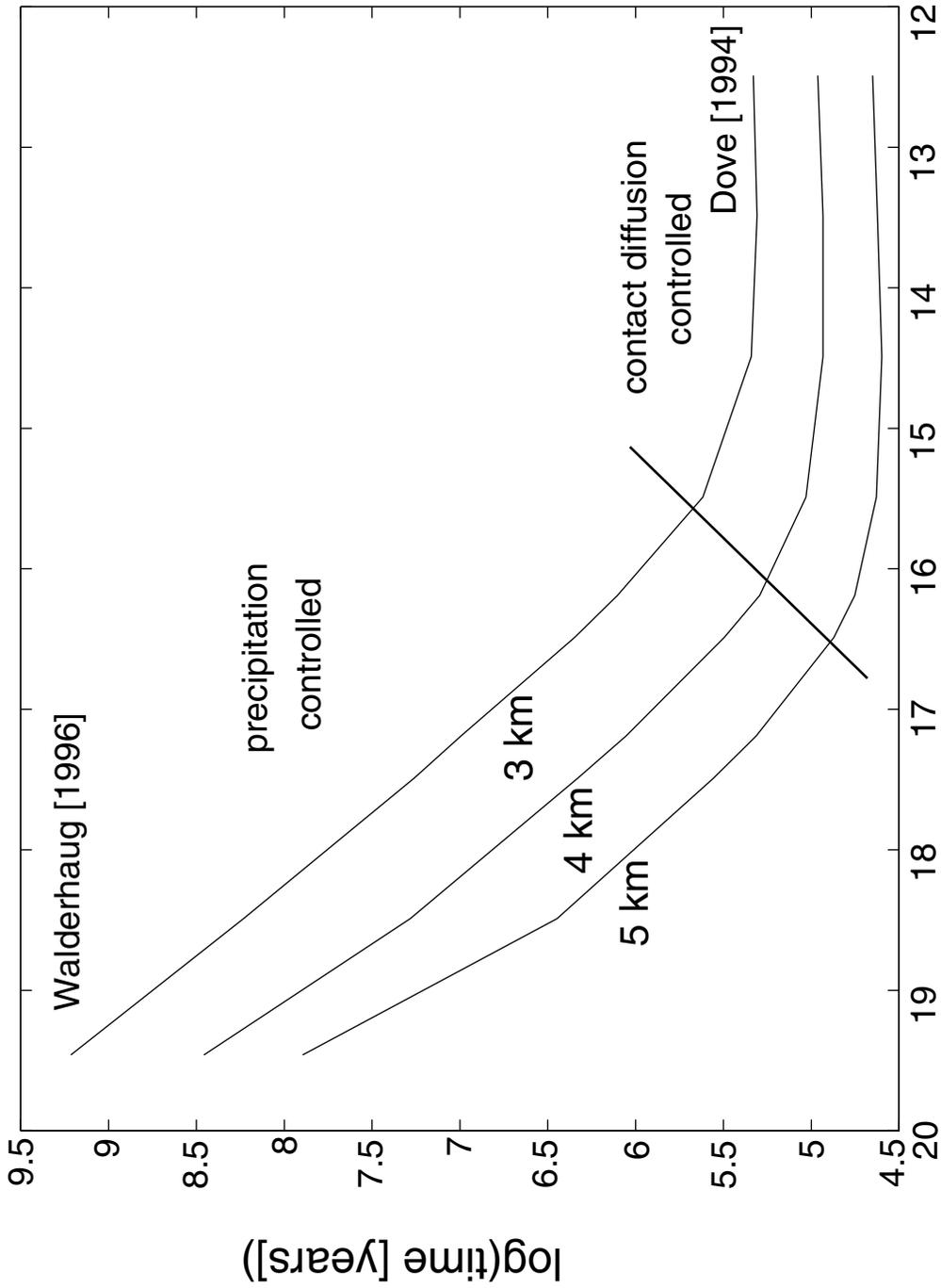
Figure 9. Timescale to close the porosity of a sandstone as a function of the kinetics constant for quartz precipitation varying between two end-members published in the literature [*Dove*, 1994; *Walderhaug*, 1996]. These simulations are performed for the same geometry as in Figure 8. The transition between diffusion-controlled and precipitation-controlled compaction (line) varies with the burial depth.

(a) porosity $t = 10$ kyrs   (b) porosity $t = 80$ kyrs   (c) porosity $t = 130$ kyrs

(d) mass diffused $t = 32$ kyrs   (e) mass diffused $t = 80$ kyrs   (f) mass diffused $t = 130$ kyrs

(g) concentration $t = 10$ kyrs   (h) concentration $t = 80$ kyrs   (i) concentration $t = 130$ kyrs

Figure 10. Compaction of a fine-grained gouge and cementation around a fracture. The whole domain is 20×20 cm. Plot (a), (b), and (c) show the porosity evolution, plot (d), (e), and (f) represent the accumulated diffusive transport, and plot (g), (h), and (i) show the concentration of dissolved silica. The small grained gouge exports silica to the fault walls which become cemented.

fracture $L_f \sim$ uniform (90, 110) micron and on the right wall $L_f \sim$ uniform (100, 120) micron. As in the previous two examples, the initial simulation domain is given as a 20 $\times$ 20 cm rock sample at 3 km burial depth.

[60] The simulation (Figure 10) clearly shows that as the gouge compacts by pressure solution it also exports some material to both sides of the fracture. The fracture compacts

due to grain indentation where the dissolved mass are transported out of the fracture and precipitates as cement along the fracture walls (Figure 10). Porosity first decreases in the fracture gouge, Figure 10h shows that the percolation threshold is reached in the gouge while diffusion is still active outside of the fracture. Due to the smaller grains in the area above the fracture, compared to the grains in the area
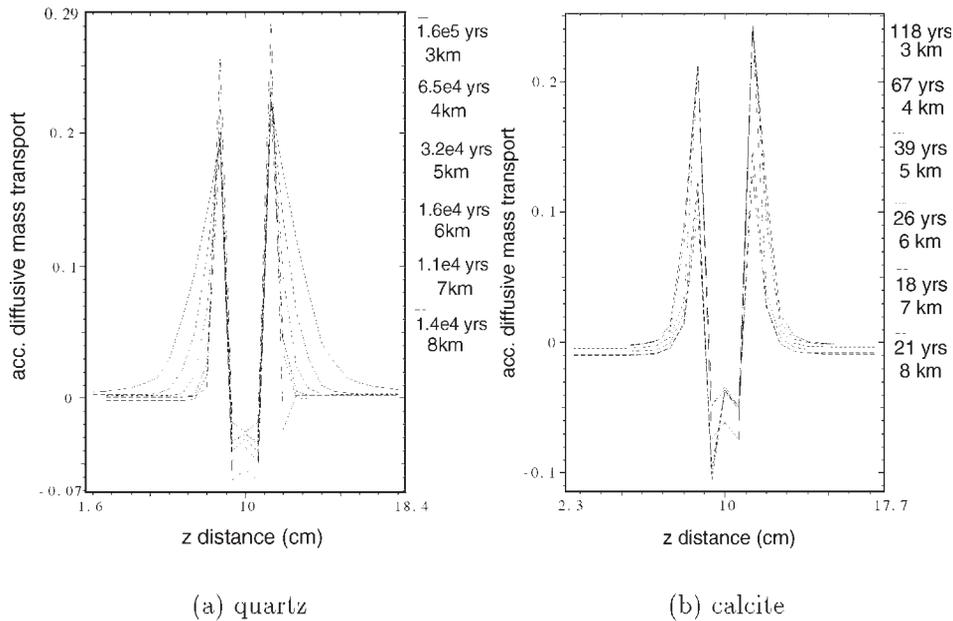
Figure 11. Accumulated mass transported by diffusion along a cross section perpendicular to the fracture of Figure 10 once the porosity of the whole system is less than 3%. The curves represented different depth conditions from 3 to 8 km. The distance over which the gouge exports material decreases with increasing depth because at greater depth, porosity closes faster than at shallow depth and therefore the duration available for transport by diffusion is shorter. This effect is stronger in the sandstone of Plot (a) than in the case of a pure limestone in Plot (b).

below, the upper domain compacts faster (see Figure 10c). The characteristic distance over which cementation occurs depends on the relative rates of reaction and diffusion in the pore space. In this example diffusion out of the contact is the rate-limiting process. For a quartz-bearing gouge, cementation typically occurs on a scale of 5 cm in the fault walls (Figure 10f).

[61] Figure 11 illustrates the accumulated mass transported by diffusion along a cross section perpendicular to the fracture of Figure 10 once the porosity of the whole system drops below 3%. Two systems are considered: pure quartz and pure calcite rocks. Each curve in the figure represents a different burial depth. For both minerals, mass is lost inside the fracture and transported into the host rock. However, in the case of calcite this diffusive mass transfer occurred over shorter distances than with quartz. This difference is probably due to the faster rate of dissolution for calcite compared to quartz. With calcite the whole process lasted for only 120 to 21 years, for burial depth ranging from 3 to 8 km, while it lasted for 161,000 to 14,000 years in the case of quartz. In this example, the timescales associated with deformation are hundred to thousands of years and are comparable to the timescales of earthquakes recurrence. Thus, to the extent that our simulations accurately represents natural fault zones.

6. Implications for Geological Systems

[62] As pressure solution is the consequence of a multistep mechanism, the derivation of a creep law requires some knowledge of the rate-controlling processes. This may change during the compaction process with varying physicochemical conditions in the rock. Moreover, during defor-

mation the grain contact surface area increases and deformation can shift from a diffusion-controlled mechanism to a surface reaction-controlled mechanism. This is why we have chosen to analyze the process by a fully coupled model that accounts for dissolution at grain contacts, diffusion along the grain boundaries to the pore, diffusion in the pore space, and precipitation on the free surfaces.

[63] All the simulations indicate how a porosity heterogeneity induces contact stress gradients which provide the driving force for local mass transport. In this model there is no need for large-scale fluid flow in the rock nor high fluid fluxes to explain how material can be transported and redistributed over distances of cm to 10s of cm. The case of a concretion with smaller or bigger grains embedded in a homogeneous porous medium undergoing pressure solution provides a simple test case to study the dynamics of coupled pressure solution at a grain scale and solute transport by diffusion. In the case of our no-flow boundary conditions, the typical distance over which this process occurs is 10 cm in pure sandstone and 5 cm in limestone.

[64] The second geometry, the development of differential cementation and compaction in layered sedimentary rocks, gives some answers to a long-going debate in sedimentology: how can cemented layers with overgrowths alternate with layers where there is strong evidence for extensive pressure solution. The fact that the initial grain sizes are different drives the system toward a state where one layer looses porosity by grain indentation (compaction) whereas in the other porosity is lost primarily by overgrowth (cementation). Because of the differences in grain size, the timescales for porosity loss are different in the two layers: aggregates of small grains loose porosity faster than

aggregates of bigger grains. Another driving force that could explain how dissolution and cementation become localized could be an initial heterogeneity in the mineralogy. For example, clay minerals are believed to enhance quartz dissolution in sandstones [*Oelkers et al.*, 1996]. If some layers of a sandstone contain more clay minerals, they would also contain a higher concentration of aqueous silica and gradients of concentration can develop between layers, causing differences in degree of cementation.

[65] Finally, in the third geometry, the fault gouge, mass transport occurs into both sides of the fracture leading to porosity loss and development of fault seals in the host rock because of cementation. The length scale for cementation varies according to mineralogy and depth, with our simulations showing mass transport on distances ranging from several cm to ~10 cm. The distance over which the transport occurs depends strongly on the duration of compaction. When the porosity closes rapidly, the time allowed for diffusion is short and transport occurs only over small distances. Mass transport over length scales > grain size lasts as long as the porosity is higher than the percolation threshold (~5%). Below this porosity, large-scale mass transport turns off and pressure solution occurs only on the scale of individual grains.

7. Conclusions

[66] When an initial heterogeneity is present in a porous medium undergoing pressure solution, the stress along grains contacts can vary spatially. This leads to gradients in solute concentration due to stress-enhanced dissolution at grain contacts and provides the driving force for mass transport between regions with different porosity and grain size. We have simulated this process for various geological examples: the cementation in and around concretions, differential compaction in sedimentary rocks, and mass transport and compaction in a fault gouge.

[67] All three examples show mass transport from areas of finer grains to areas of larger grains as the areas with finer grains compact faster than the ones with larger grain sizes. When the porosity in some area is less than 5%, the percolation threshold has been reached and pressure solution will then only occur on the scale of individual grains in that area. In all simulations the percolation threshold was first reached in the areas containing the fine grains. Then large-scaled diffusive mass transport only occurs within the coarser grain-sized material, driven by a nonuniform distribution of grain size. The porosity becomes equalized at about 3% in the entire rock volume as diffusive mass transfers essentially ceases.

[68] In the case of a concretion containing larger grains than the surroundings, the concretion behaves almost as a stiff region and most of the deformations is taken up by the surroundings. In the opposite case, with a small-grained concretion in the middle of an area consisting of larger grains, our simulations show that the concretion shrinks.

[69] With a model where boundary conditions as well as other governing parameters can change, chemical compaction in a monomineralic system, driven by the increase of solubility at grain contacts was tested at different depths. We found that precipitation should be the rate-limiting process in the case of silicate minerals such as quartz at shallow depths (2–5 km) while diffusive transport should be the rate-limiting process for minerals like carbonates or quartz at greater depth. At this stage the model has only been treated for cases where stress, temperature, and pore fluid pressure are kept constant. The inclusion of depth and temperature dependent variables as well as fluid flow would be a natural extensions of our model.

[70] Geological environments where evidence for a local diffusive mass transport have been observed could behave according to this model of coupled pressure solution and diffusion. In such systems, there is no need for a fluid flow over large distances to explain locally observed variations in porosity or overgrowth density. Such processes could apply during compaction of sediments as well as in the surroundings of an active fault where production of fine-grained gouge during earthquakes could continually renew the porosity.

References

Berner, R. A., Rate of concretion growth, *Geochim. Cosmochim. Acta*, *32*, 447–483, 1968.

Bjørkum, P. A., How important is pressure solution in causing dissolution of quartz in sandstones?, *J. Sediment. Res.*, *66*, 147–154, 1996.

Bjørkum, P. A., and O. Walderhaug, Geometrical arrangement of calcite cementation within shallow marine sandstones, *Earth Sci. Rev.*, *29*, 145–161, 1990.

Bjørlykke, K., and P. K. Egeberg, Quartz cementation in sedimentary basins, *AAPG Bull.*, *77*, 1538–1548, 1993.

Caron, J. M., J. L. Potdevin, and E. Sicard, Solution-deposition processes and mass transfer of a minor fold, *Tectonophysics*, *135*, 77–86, 1987.

Cox, S. F., and M. S. Paterson, Experimental dissolution-precipitation creep in quartz aggregates at high temperatures, *Geophys. Res. Lett.*, *78*, 1401–1404, 1991.

de Boer, R. B., P. Nagtegaal, and E. Duyvis, Pressure solution experiments on quartz sand, *Geochim. Cosmochim. Acta*, *41*, 257–264, 1977.

Dewers, T., and P. Ortoleva, A coupled reaction/transport/mechanical model for intergranular pressure solution stylolites, and differential compaction and cementation in clean sandstones, *Geochim. Cosmochim. Acta*, *54*, 1609–1625, 1990.

Dove, P. M., The dissolution kinetics of quartz in sodium chloride solutions at 25°C to 300°C, *Am. J. Sci.*, *294*, 665–712, 1994.

Evans, J. P., and F. M. Chester, Fluid-rock interactions in faults of the San Andreas system: Inferences from San Gabriel fault rock geochemistry and microstructures, *J. Geophys. Res.*, *100*, 13,007–13,020, 1995.

Feder, J., *Fractals*, Plenum, New York, 1988.

Gaviglio, P., M. Chaye d'Albissin, F. Bergerat, and S. Vandycke, Modifications de texture dans la craie au contact de failles normales: Un exemple de graben dans le bassin de Mons (Belgique), *Bull. Soc. Geol. Fr.*, *164*, 565–575, 1993.

Gratier, J. P., Le fluage des roches par dissolution-cristallisation sous contrainte dans la croûte supérieure, *Bull. Soc. Geol. Fr.*, *164*, 267–287, 1993a.

Gratier, J. P., Experimental pressure solution of halite by an indenter technique, *Geophys. Res. Lett.*, *20*, 1647–1650, 1993b.

Gratier, J. P., and R. Guiguet, Experimental pressure solution-deposition on quartz grains: The crucial effect of the nature of the fluid, *J. Struct. Geol.*, *8*, 845–856, 1986.

Gratier, J. P., and L. Jenatton, Deformation by solution-deposition and reequilibration of fluid inclusions in crystals depending on temperature, internal pressure, and stress, *J. Struct. Geol.*, *6*, 189–200, 1984.

Hazidazeh, J., and F. F. Foit, Feasibility of estimating cementation rates in a brittle fault zone using Sr/Ca partition coefficients for sedimentary diagenesis, *J. Struct. Geol.*, *22*, 401–409, 2000.

Heidari, E., and C. H. Moore, Zonation and geochemical patterns of burial calcite cements: Upper Smackover formation, Clarke County, Mississippi, *J. Sediment. Petrol.*, *63*, 44–60, 1993.

Heidug, W. K., Intergranular solid-fluid phase transformations under stress: The effect of surface forces, *J. Geophys. Res.*, *100*, 5931–5940, 1995.

Heydari, E., Porosity loss, fluid flow, and mass transfer in limestone reservoirs: Application to the upper Jurassic Smackover formation, Mississippi, *AAPG Bull.*, *84*, 100–118, 2000.

Hickman, S. H., and B. Evans, Experimental pressure solution in halite — The effect of grain interphase boundary structure, *J. Geol. Soc. (London)*, *148*, 549–560, 1991.

Hickmam, S. H., and B. Evans, Kinetics of pressure solution at halite-silica interfaces and intergranular clay films, *J. Geophys. Res.*, *100*, 13,113–13,132, 1995.

Israelachvili, J. N., Measurements of the viscosity of liquids in very thin films, *J. Colloid Interface Sci.*, *110*, 263–271, 1986.

Janssen, C., W. Michel, M. Bau, V. Luders, and K. Muhle, The North Anatolian Fault Zone and the role of fluids in seismogenic deformation, *J. Geol.*, *105*, 38–403, 1997.

Kamb, W. B., Theory of preferred crystal orientations developed by crystallization under stress, *J. Geol.*, *67*, 153–170, 1959.

Langtangen, H. P., *Computational Partial Differential Equations*, Springer-Verlag, New York, 1999.

Lasaga, A. C., *Kinetic Theory in the Earth Sciences*, Princeton Univ. Press, Princeton, N. J., 1998.

Lehner, F. K., A model for intergranular pressure solution in open systems, *Tectonophysics*, *245*, 153–170, 1995.

Mair, K., and C. Marone, Friction of simulated fault gouge for a wide range of velocities and normal stresses, *J. Geophys. Res.*, *104*, 28,899–28,914, 1999.

Malmstrom, M. E., G. Destouni, S. A. Banwart, and B. H. E. Stromberg, Resolving the scale-dependence of mineral weathering rates, *Environ. Sci. Technol.*, *34*, 1375–1378, 2000.

McBride, E. F., Quartz cement in sandstones: A review, *Earth Sci. Rev.*, *26*, 69–112, 1989.

Merino, E., Self-organization in stylolites, *Am. Sci.*, *80*, 466–473, 1990.

Merino, E., P. Ortoleva, and P. Strickholm, Generation of evenly-spaced pressure-solution seams during (late) diagenesis: A kinetic theory, *Contrib. Mineral. Petrol.*, *82*, 360–370, 1983.

Mullis, A. M., Determination of the rate-limiting mechanism for quartz pressure dissolution, *Geochim. Cosmochim. Acta*, 1993.

Nakashima, S., Diffusivity of ions in pore water as a quantitative basis for rock deformation rate estimates, *Tectonophysics*, *245*, 185–203, 1995.

Oelkers, E. H., P. A. Bjørkum, and W. M. Murphy, A petrographic and computational investigation of quartz cementation and porosity reduction in North Sea sandstones, *Am. J. Sci.*, 1996.

Oelkers, E. H., P. A. Bjørkum, P. H. Nadeau, and W. M. Murphy, Making diagenesis obey thermodynamics and kinetics: The case of quartz cementation in sandstones from offshore mid-Norway, *Appl. Geochem.*, *15*, 295–309, 2000.

Pashley, R. M., and J. N. Israelachvili, Molecular layering of water in thin films between mica surfaces and its relation to hydration forces, *J. Colloid Interface Sci.*, *101*, 510–522, 1984.

Pashley, R. M., and J. A. Kitchener, Surface forces in adsorbed multilayers of water on quartz, *J. Colloid Interface Sci.*, *71*, 491–500, 1979.

Paterson, M. S., Nonhydrostatic thermodynamics and its geologic applications, *Rev. Geophys. Space Phys.*, *11*, 355–389, 1973.

Plummer, L. N., and E. Busenberg, The solubilities of calcite, aragonite, and vaterite in CO_2-H_2O solutions between 0 and 90°C, and an evaluation of the aqueous model for the system $CaCO_3$-CO_2-H_2O., *Geochim. Cosmochim. Acta*, *46*, 1011–1040, 1982.

Plummer, L. N., T. L. M. Wigley, and D. L. Parkhurst, The kinetics of calcite dissolution in CO_2-water systems at 5° to 60°C and 0.0 to 1.0 atm CO_2, *Am. J. Sci.*, *278*, 179–216, 1978.

Railsback, L. B., Evaluation of spacing of stylolites and its implications for self-organization of pressure solution, *J. Sediment. Res.*, *68*, 2–7, 1998.

Raiswell, R., The growth of Cambrian and Liassic concretions, *Sedimentology*, *17*, 147–171, 1971.

Raj, R., Creep in polycrystalline aggregates by matter transport through a liquid phase, *J. Geophys. Res.*, *87*, 4731–4739, 1982.

Renard, F., and P. Ortoleva, Water films at grain-grain contacts: Debye-Huckel, osmotic model of stress, salinity and mineralogy dependence, *Geochim. Cosmochim. Acta*, *61*, 963–970, 1997.

Renard, F., P. Ortoleva, and J. P. Gratier, Pressure solution in sandstones: Influence of clays and dependence on temperature and stress, *Tectonophysics*, *280*, 257–266, 1997.

Renard, F., P. Ortoleva, and J. P. Gratier, An integrated model for transitional pressure solution in sandstones, *Tectonophysics*, *312*, 97–115, 1999.

Renard, F., J. P. Gratier, and B. Jamtveit, Kinetics of crack-sealing, intergranular pressure solution, and compaction around active faults, *J. Struct. Geol.*, *22*, 1395–1407, 2000.

Rutter, E. H., The kinetics of rock deformation by pressure solution, *Philos. Trans. R. Soc. London*, *283*, 203–219, 1976.

Schneider, F., Mechanical and chemical compaction model for sedimentary basin simulators, *Tectonophysics*, *263*, 307–317, 1996.

Schutjens, P. M. T., Experimental compaction of quartz sand at low effective stress, *J. Geol. Soc. (London)*, *148*, 527–539, 1991.

Shimizu, I., Kinetics of pressure solution creep in quartz: Theoretical considerations, *Tectonophysics*, *245*, 121–134, 1995.

Spiers, C. J., and R. H. Brzesowsky, Densification behaviour of wet granular salt: Theory versus experiment, *Symp. Salt*, *1*, 83–91, 1993.

Trewin, N. H., and A. E. Fallick, Quartz cement origins and budget in the Tumblagooda sandstone, Western Australia, in *Quartz Cementation in Sandstones*, edited by R. H. Worden and S. Morad, Blackwell Sci., Malden, Mass., 2000.

Walderhaug, O., Kinetic model of quartz cementation and porosity loss in deeply buried sandstone reservoirs, *AAPG Bull.*, *80*, 731–745, 1996.

Weyl, P. K., Pressure solution and the force of crystallization — a phenomenological theory, *J. Geophys. Res.*, *69*, 2001–2025, 1959.

Worden, R. H., and S. Morad, Quartz cementation in oil field sandstones: A review of key controversies, in *Quartz Cementation in Sandstones*, edited by R. H. Worden and S. Morad, Blackwell Sci., Malden, Mass., 2000.

————————————

K. Bjørlykke, E. Gundersen, and B. Jamtveit, Institute of Geology, University of Oslo, Box 1047 Blindern, 0316 Oslo, Norway. (ueg@geologi.uio.no)

D. K. Dysthe, Department of Physics, University of Oslo, Box 1046 Blindern, 0316 Oslo, Norway. (d.k.dysthe@fys.uio.no)

F. Renard, LGIT, Observatoire de Grenoble, BP 53, 38041 Grenoble, France. (frenard@lgit.obs.ujf-grenoble.fr)